Next Materials 2 (2024) 100067

Contents lists available at ScienceDirect

Next Materials

journal homepage: www.sciencedirect.com/journal/next-materials

Research article

In-gap states and local structures around substitutional defects in La- or Nb-doped n-type $SrTiO_3$

Rei Akasegawa [a], Kan Hachiya [a,b,*], Takashi Sagawa [a,b]

[a] Department of Fundamental Energy Science, Graduate School of Energy Science, Kyoto University, Yoshida-honmachi, Sakyo-ku, Kyoto 606-8501, Japan
[b] Integrated Research Center for Carbon Negative Science, Institute of Advanced Energy, Kyoto University, Gokasho, Uji, Kyoto 611-0011, Japan

ARTICLE INFO

Keywords:
Strontium titanate
Electron doping
In-gap states
Substitutional defects

ABSTRACT

First-principles calculations with DFT+*U* method were conducted on the local structures and the in-gap electronic states of n-type $SrTiO_3$, whose electron doping was realized by substitution of Sr by La or Ti by Nb. For both La-doped and Nb-doped $SrTiO_3$, cubic structures were proved to be stable e3ven when tetragonal structures were assumed, as suggested also in a reported experimental study. In La-doped $SrTiO_3$, O atoms neighboring the substitutional La were symmetrically attracted toward the dopants. Sharp electron band observed at the top of the bandgap, which gave n-type conductivity and resulted from the intersection of Fermi energy level at the conduction band bottom with La-doping, was composed of 3*d* orbitals in Ti. The La-doping transformed some of the *p* electrons in O into the *d* electrons in Ti in the sharp band, and these electrons at Fermi level were expected to act as n-type carriers. In Nb-doped $SrTiO_3$, on the other hand, Ti atoms at the first, second and third nearest neighbors of the Nb, which were in the same Ti-O plane surrounding the dopants, were repelled away from the Nb dopants to be isotropic local expansion, while O atoms neighboring Nb were attracted toward the dopants in the expanded local structure. Sharp band of the in-gap states just below the Fermi energy of the Nb-doped $SrTiO_3$ was not only of the 3*d* orbitals in the first nearest-neighbor Ti atoms, but also of those in the second and third nearest-neighbor Ti atoms of the dopants. The degree of Fermi level intrusion into conduction band and atomic rearrangements near Nb substitutions were milder than those of La substitutions. As replacement of Sr atoms by La not contained in Ti-O network does not disturb the electron transport within Ti-O conduction planes, Nb-doping in Ti site does not interrupt the n-type carrier transportation even though Nb atoms are in Ti-O network, because of the formation of conduction path which bypasses the unit cell containing the dopants.

1. Introduction

A typical wide-gap semiconductor, $SrTiO_3$, has a bandgap of 3.2 eV [1]. As for the n-type doping of the $SrTiO_3$, La-doped $SrTiO_3$ (La:$SrTiO_3$) and Nb-doped $SrTiO_3$ (Nb:$SrTiO_3$) are well-known, and they are among the key materials in the oxide electronics [2]. The electron-dope mechanism to induce n-type conductivity in $SrTiO_3$ is widely investigated [3–7]. A wide variety of the electronic, thermoelectric and optical properties are emerged through electron doping, and it is accomplished by substitution of La to Sr, or Nb to Ti. Nature of in-gap states, which are defined as localized states emergent in the energy gap between conduction and valence bands introduced by doping [8,9], is especially important to discuss the type of conduction, whether it is classified as a polaron conduction or not, for example [10]. Electron doping is also enabled by introduction of O vacancy, and it is confirmed and investigated by a simulation [11]. In this context, both experimental and computational approaches have been taken to clarify the bandgap electronic states, which arise as an effect of the substitution of cations with dopants. Another study with the ab-initio electronic structure calculations for La- or Nb-doped STO were performed by Wunderlich et al. [12]. They investigated the doping effect through estimation of the effects of dopant concentrations and lattice volumes on the effective mass of the carriers in the crystal.

Recently, an experimental study putting an emphasis on the in-gap states and local structures around dopants have been made on the La- or Nb-doped n-type $SrTiO_3$ [8]. It proved that O ions around the dopants are attracted toward the substituted ions, and the conduction band bottoms are intersected by Fermi energy level to produce sharp

---

* Corresponding author at: Department of Fundamental Energy Science, Graduate School of Energy Science, Kyoto University, Yoshida-honmachi, Sakyo-ku, Kyoto 606-8501, Japan.

E-mail address: hachiya.kan.3v@kyoto-u.ac.jp (K. Hachiya).

https://doi.org/10.1016/j.nxmate.2023.100067
Received 22 September 2023; Received in revised form 8 November 2023; Accepted 9 November 2023

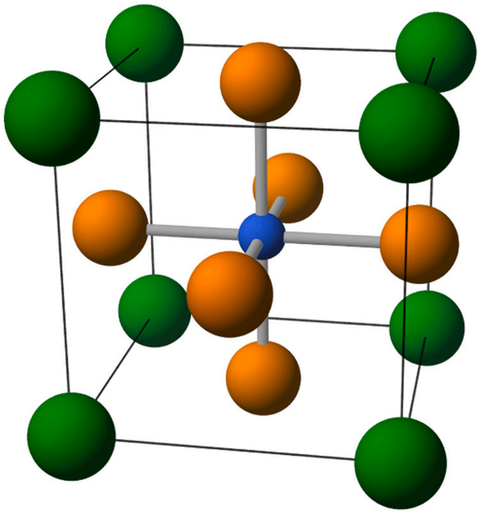

Fig. 1. Schematics for the unit cells of cubic $SrTiO_3$ used for the simulations for $La{:}SrTiO_3$ and $Nb{:}SrTiO_3$. The Sr, Ti and O atoms are colored with green, blue and orange, respectively.

in-gap-state bands. The in-gap-state bands can be observed with, such as, photoelectron spectroscopy [8,13]. The emergence of such bands, which are positioned just under the Fermi energy level, results from local lattice distortion introduced by the La/Nb substitution for electron doping and should lead to n-type conductivity. It is also confirmed that the La-doping hardly transforms cubic lattice of undoped $SrTiO_3$ into tetragonal structure, and slightly introduce local lattice distortion around the substitutional defects to generate symmetrical displacement of the nearest-neighbor O atoms toward the dopant ions [8]. Therefore, such transformation or distortion hardly alter the symmetry. This is consistent with the fact that the Raman activities of the vibrational modes in cubic $SrTiO_3$ is scarcely altered by doping [14].

In typical metal oxide perovskites, charge carriers for the p- or n-type semiconductors by doping or by oxygen deficiency conduct in (002) and its equivalent planes composed of metal and oxygen ions [8,15], in order to exhibit functionality through high mobility. In-gap electronic states introduced by hole or electron doping should be organized by the orbitals in metal or oxygen ions and their hybridizations, because metal-oxygen network in the plane can be the conduction path.

In the present study, we perform first-principles calculations on the La- or Nb-doped n-type $SrTiO_3$ to investigate the local structures and in-gap electronic structures induced by electron doping. The distorted lattice around the substitutional dopants are reproduced, and the components of the sharp in-gap-state bands just below the Fermi energy level are analyzed.

2. Computational details

Quantum ESPRESSO program suite [16,17], version 6.6, was used for the electronic structure and lattice structure relaxation calculations. The density functional theory (DFT) within the generalized-gradient approximation (GGA) [18] was chosen. With the Hubbard U correction named as the DFT+U method [19,20], we intended to improve the prediction of the electronic structure around bandgap and the local structures. In this study, the correction with $+U$ was applied only to Ti atoms.

As for the pseudopotentials, PSlibrary [21] was used. The Projected Augmented Wave (PAW) type [22] pseudopotential files for the revised PerderBurke-Ernzerhof (PBE) exchange-correlation functionals for solids (PBEsol) [23] were selected for Sr (Sr.pbesol-spn-kjpaw psl.1.0.0. UPF), Ti (Ti.pbesol-spnkjpaw psl.1.0.0. UPF) and O (O.pbesol-n-kjpaw psl.1.0.0. UPF), respectively. As for La and Nb, however, the PBEsol files are not provided. We used psudopotential files for PBE [24] instead (La. pbe-spfn-kjpaw psl.1.0.0. UPF, Nb.pbe-spn-kjpaw psl.1.0.0. UPF) for the PBEsol functional calculations by specifying ‘input dft = pbesol’ [25]. Kinetic energy cutoff for wavefunctions (‘ecutwfc’) and for charge density and potential (‘ecutrho’) were set to the largest values among those suggested in the PBEsol pseudopotential files specified above, which were ‘ecutwfc = 52′ Ry and ‘ecutrho = 576′ Ry.

Table 1
Calculated direct gap at Γ point (E_0), indirect bandgap between valence band top at R and conduction band bottom at Γ points (E_g) and lattice constant for cubic $SrTiO_3$ (a) for U in DFT+U method. Experimental values (Expt.) for E_0, E_g [27] and a [28] are also presented.

U (eV)	E_0 (eV)	E_g (eV)	a (Å)
0	2.18	1.85	3.892
2.0	2.34	1.98	3.900
3.0	2.41	2.05	3.904
4.0	2.52	2.13	3.908
5.0	2.63	2.23	3.912
6.0	2.77	2.34	3.918
7.0	2.92	2.48	3.923
8.0	3.10	2.54	3.931
8.8	3.28	2.80	3.937
9.0	3.29	2.81	3.939
9.2	3.23	2.74	3.941
9.5	3.15	2.65	3.945
10.0	3.02	2.51	3.950
Expt.	3.75	3.25	3.905

Simulation supercells were constructed by assembling unit cells illustrated in Fig. 1. For $La{:}SrTiO_3$, $2 \times 2 \times 2$ unit cells ($Sr_8Ti_8O_{24}$) were used, and Sr atom at the center of the supercell was substituted with La atom. For $Nb{:}SrTiO_3$, $3 \times 3 \times 3$ unit cells ($Sr_{27}Ti_{27}O_{81}$) were used, and Ti atom at the center was substituted with Nb. As we will discuss later, these cell sizes are the minimum to investigate into the atomic coordinations and their relaxations which accompany La- or Nb-doping, and the electronic structures including those of the Ti-O planes surrounding the substitutional defects above under periodic boundary condition. The lattice planes are indicated as those for the unit cell in Fig. 1. All faces of the unit cell in Fig. 1 are (100) and its equivalent planes, and those of Ti and O are (200) and its equivalent planes. Preliminary calculations with undoped $SrTiO_3$ were executed for the single unit cell.

The k-point sampling grids with Monkhorst-Pack method [26] of $6 \times 6 \times 6$ k points were used for the undoped crystal calculation, and $3 \times 3 \times 3$ k points were used for the larger supercells for the doped crystals. The total energy convergence criterion for self-consistent field (SCF) calculations was 1.0×10^{-6} Ry for supercell. The structural optimizations were performed until atomic forces were smaller than 1.0×10^{-4} Ry. All atoms in the supercell were relaxed to find the optimized structure during calculations for the La or Nb substitution. Cubic structure was assumed for the undoped $SrTiO_3$, while tetragonal structures were assumed for the La- or Nb-doped $SrTiO_3$.

3. Results and discussions

3.1. Calculations for $SrTiO_3$

In order to optimize the value of U in DFT+U method, the lattice

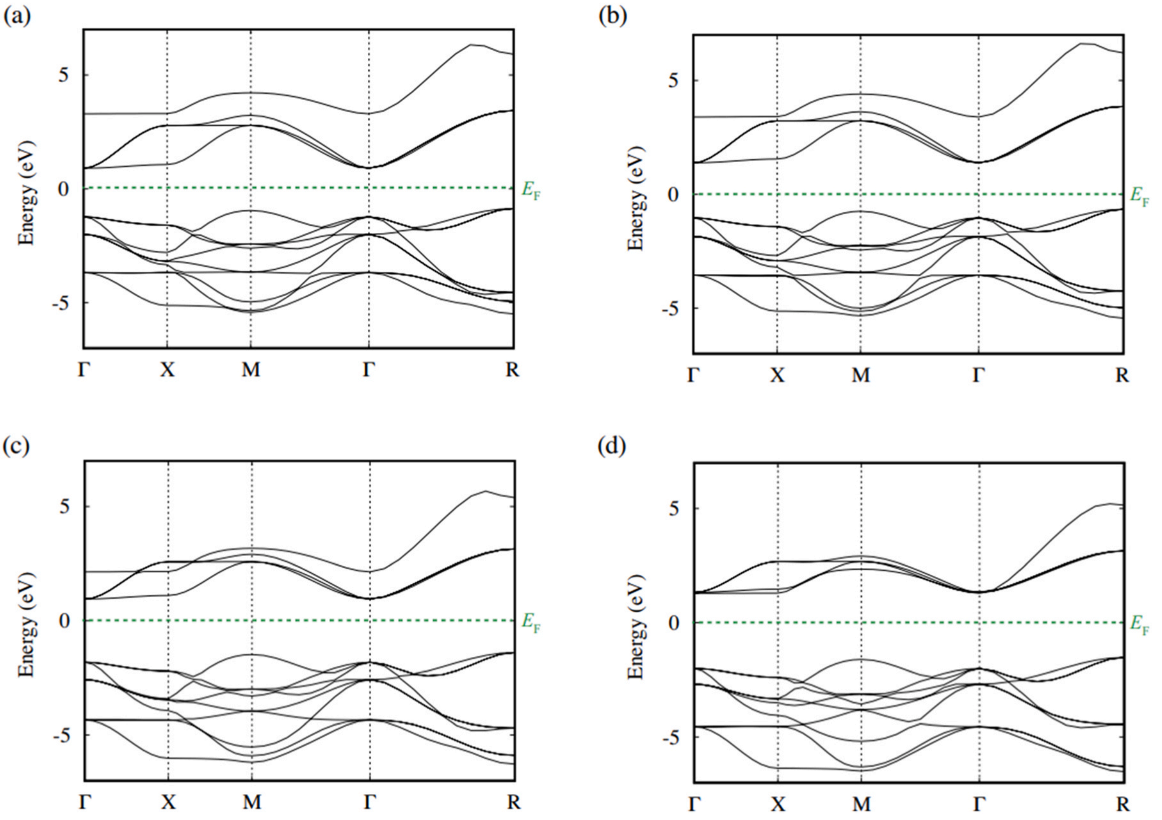

Fig. 2. Band structures for cubic SrTiO3 calculated with DFT+U method: U = (a) 0, (b) 3.0, (c) 6.0 and (d) 9.0 eV. Fermi energy (E_F) is set to the origin of energy.

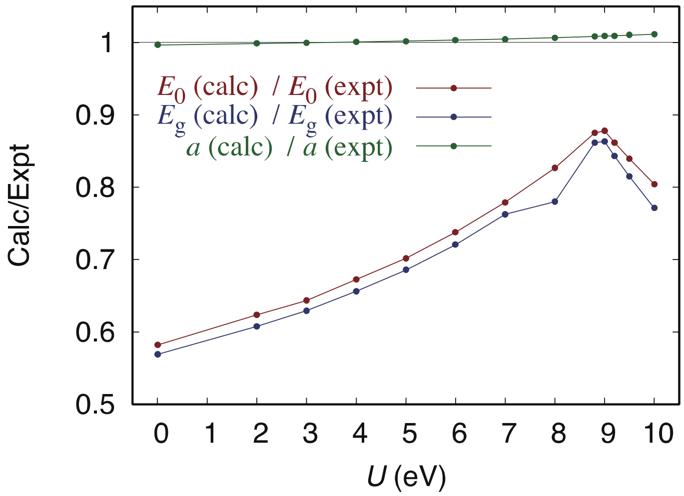

Fig. 3. Calculated direct gap at Γ point (E_0), indirect bandgap between valence band top at R and conduction band bottom at Γ points (E_g) and lattice constant for cubic $SrTiO_3$ (a) compared with experimental values for U in DFT+U method. The ratio of the calculated values to the corresponding experimental values are indicated.

Table 2
L̈owdin charges for the atoms in the relaxed local structure of $SrTiO_3$ for $U = 0$, 3.0, 6.0, 9.0.

U (eV)		Sr	Ti	O
0	total	8.79	10.26	6.89
	s	2.23	2.28	1.68
	p	6.58	5.99	5.21
	d	0.00	1.99	0.00
3.0	total	8.80	10.21	6.91
	s	2.23	2.29	1.68
	p	6.57	5.99	5.23
	d	0.00	1.93	0.00
6.0	total	8.80	10.13	6.93
	s	2.23	2.29	1.68
	p	6.57	5.99	5.25
	d	0.00	1.85	0.00
9.0	total	8.82	10.03	6.95
	s	2.24	2.29	1.68
	p	6.58	5.99	5.27
	d	0.00	1.75	0.00

constant, a, obtained in the structural relaxation and the electronic band structure for the relaxed structure, especially direct (E_0) and indirect energy gaps (E_g), were calculated and confirmed. Results are summarized in Table 1 and in Figs. 2 and 3. The calculated lattice constant for the relaxed structure was close to the experimental value at around $U = 3.0$ eV. On the other hand, the values for E_0 and E_g reached to their extrema and were the closest to the experimental values at $U = 9.0$ eV. For all the values of U, indirect bandgaps were for the R to Γ transitions, which were consistent with those observed in the experimental study [27]. A reported study for the undoped $SrTiO_3$ by DFT+U with PBE instead of PBEsol [29] did not have such extrema up to $U \leq 14.5$ eV with an overestimation of the lattice constant even at $U = 0$. Another report with PBE [30] improved the bandgap estimation with a smaller U of 6.0 eV on Ti, while the authors chose to assign extra uncommon U of 3.0 eV on Sr, which is not a transition element. Dependence of the band structure on U in PBE+U method was investigated to study La:$SrTiO_3$, and confirmed that the extremum to give a better prediction of the bandgap was at $U = 7.5$ eV [31]. Some reports claimed that too large U caused emergence of unreal bandgap states in the bandgap when applied to anatase TiO_2, and recommended $U \leq 3.0$ eV [32]. There was also a calculation for $SrTiO_3$ with a smaller U, such as 3.0 eV, with PBE+U or LDA+U [33]. Nevertheless, as we have seen in Fig. 2, no unreal mid-gap states were observed in our calculations. It is therefore no reason to choose the U of inferior prediction at anywhere along the way to reach the maximum of the bandgap energy (E_g), especially when the best prediction is obtained at its extremum as we see in Fig. 3. In the present study, the DFT+U calculations were performed not only at $U = 9.0$ eV, but also at 0, 3.0 and 6.0 eV, in order to make comparison with other reports.

The calculated L̈owdin charges [34,35] are compiled in Table 2. Initial charges (number of valence electrons) are Sr: 10.00(4 *s*: 2.00; 5 *s*: 2.00; 4*p*: 6.00); Ti: 12.00(3 *s*: 2.00; 4 *s*: 2.00; 3*p*: 6.00; 3*d*: 2.00) and O: 6.00 (2 *s*: 2.00; 2*p*: 4.00), respectively, which are defined in the pseudopotential library files. Qualitatively, increase of charge number means negativity of atoms, while decrease means positivity.

The calculated total and partial density of states are presented in

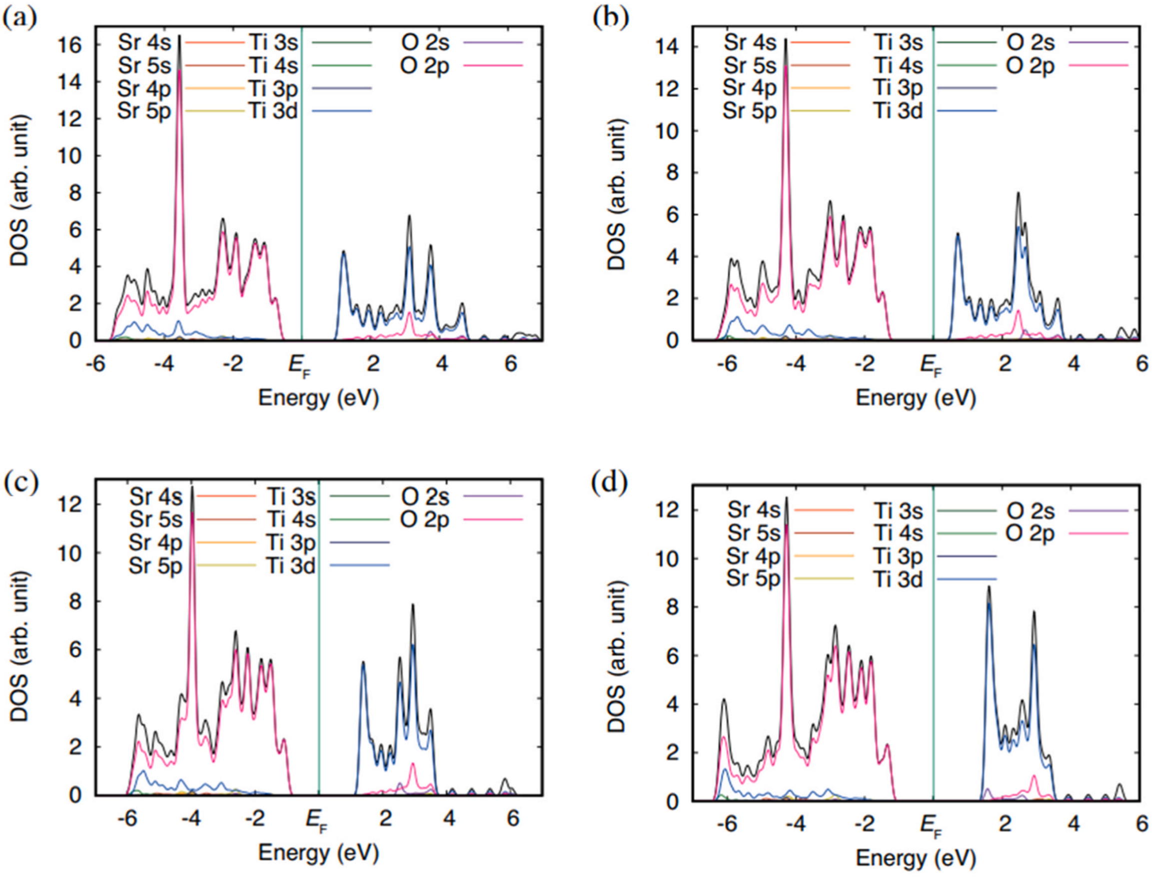

Fig. 4. Total and partial density of states for $SrTiO_3$ calculated with DFT+U method for $U =$ (a) 0, (b) 3.0, (c) 6.0 and (d) 9.0 eV. Total density of states is drawn in solid black line, and partial density of states are labeled in legend.

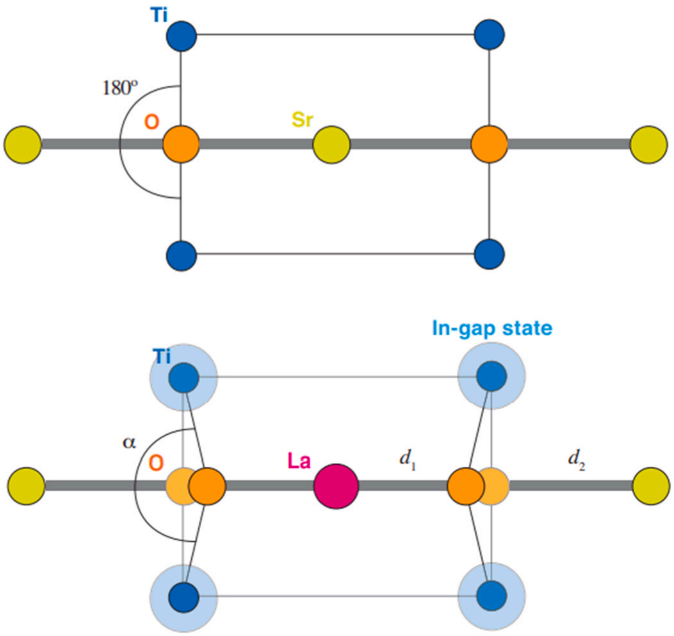

Fig. 5. Schematics for the atomic arrangements in a (110) plane around a Sr replaced by La (upper panel) before and (lower panel) after the doping.

Fig. 4. For all U except $U = 9.0$ eV, conduction band bottoms were composed of Ti 3d orbitals. At $U = 9.0$ eV, Ti 3d orbitals were hybridized with O 2s orbitals. The valence band tops were composed of O 2p orbitals.

3.2. Calculations for La:SrTiO$_3$

Although La is one of the lanthanoid, the 4f orbital of the element is empty. Therefore, it is not common to assign non-zero U to this element in DFT+U method unlike other lanthanoid elements. We confirmed U of 0, 3.0, 6.0, 9.0 eV, which were assigned only to Ti. The parameters to describe atomic arrangements around the dopant La atoms are defined in Fig. 5. The band structures are given in Fig. 6, and presented in Fig. 7 are the calculated total and partial density of states corresponding to the band structures. The in-gap states emergent with La-doping are also displayed as those localized around Ti in Fig. 5, which are evident from band structure and density of states as we see later. Results of the relaxation of atomic positions and lattice parameters to investigate the local structure around La substitutional defects is compiled in Table 3. Even though we have assumed tetragonal structure for the unit cell, cubic structure, $a = c$, was obtained through structural relaxation calculation. Therefore, we used the lattice constant of a only. The angle and the distances indicate that the O atoms neighboring the substitutional La slightly moved toward the dopants. The reported parameters were 2.719 Å (EXAFS, 20 K) or 2.761 Å (XRD, room temperature) for the Sr-O distance, 2.533 Å (EXAFS, 20 K) for the La-O distance, and ~ 170° for the angle α in Fig. 5 which was estimated from the distances at 20 K derived with EXAFS [8]. The lattice constants for a and c were 3.906 Å and 3.907 Å derived with Rietveld analysis of the XRD spectra [8]. The $a/\sqrt{2}$ was 2.762 Å for that value.

The band structures in Fig. 6 and the calculated total and partial density of states in Fig. 7 show that the Fermi energy level crossed the conduction band bottoms as an effect of the La-doping. Such electronic structure gives n-type conductivity of electrons near Fermi energy in SrTiO$_3$. The intersection of Fermi energy level at conduction band bottom yields a sharp band in photoelectron spectroscopy observed at the

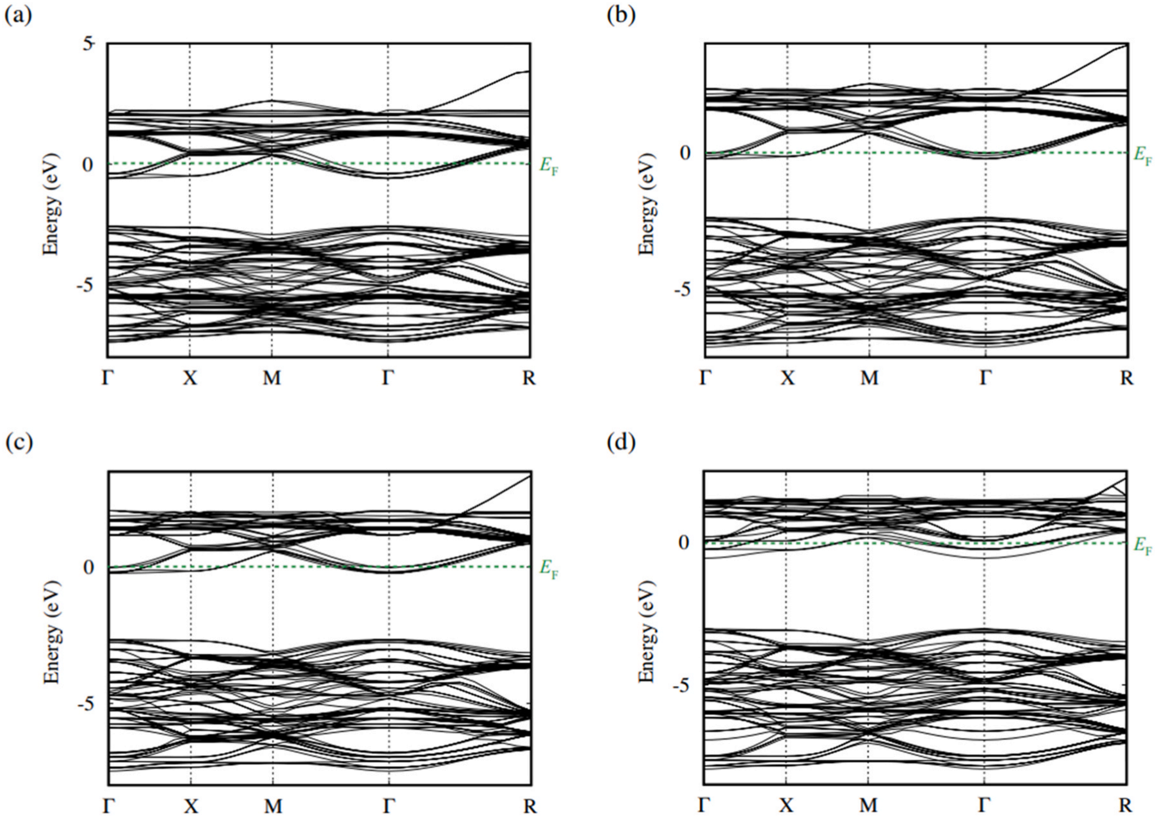

Fig. 6. Band structures for La:SrTiO$_3$ calculated with DFT+U method using a simulation box of 2 × 2 unit cells: U = (a) 0, (b) 3.0, (c) 6.0 and (d) 9.0 eV. Fermi energy (E_F) is set to the origin of energy.

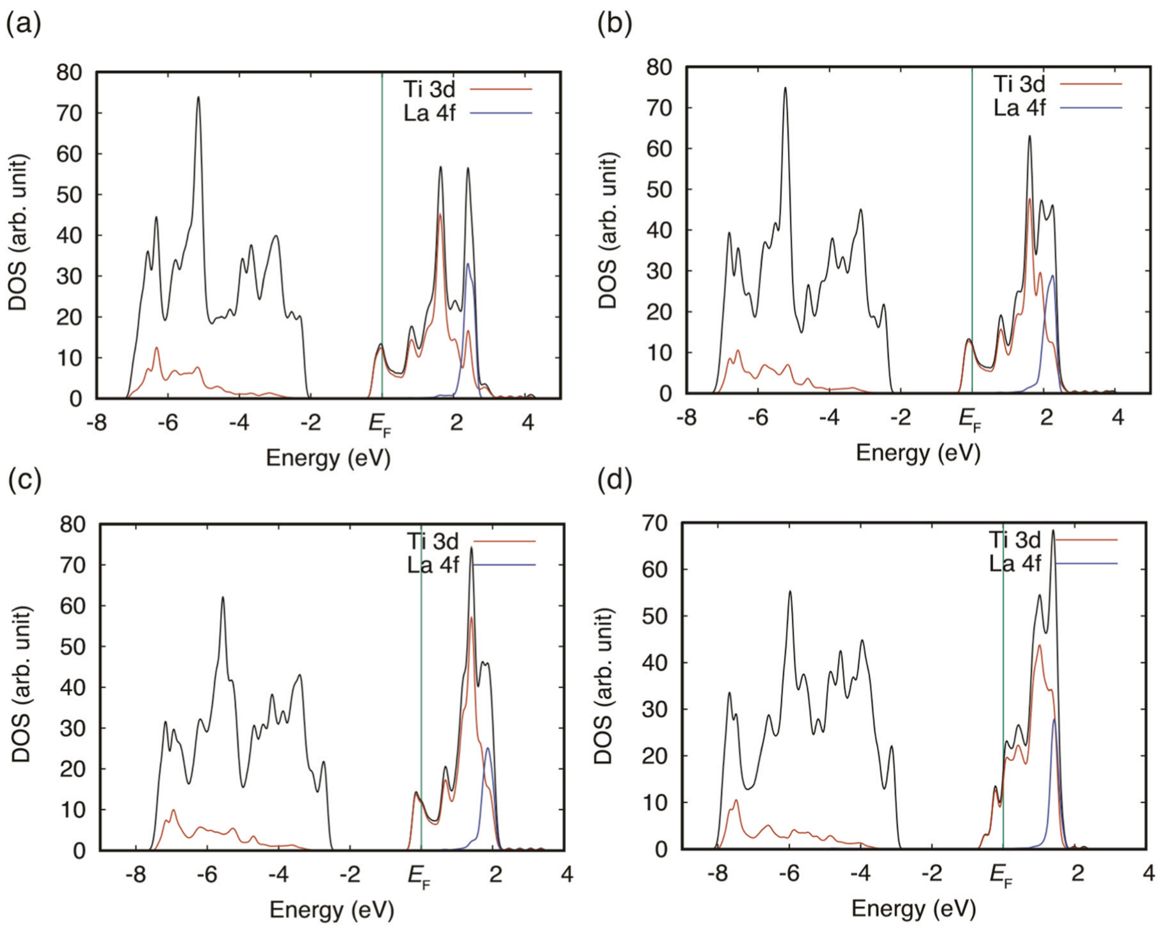

Fig. 7. Total and partial density of states for La:SrTiO$_3$ calculated with DFT+U method using a simulation box of 2 × 2 unit cells: U = (a) 0, (b) 3.0, (c) 6.0 and (d) 9.0 eV. Total density of states is drawn in solid black line, and partial density of states are labeled in legend.

Table 3
Parameters for the relaxed local structure around doped La in La:SrTiO$_3$. The angle (α) and the distances (d_1, d_2) are defined in Fig. 5.

U (eV)	α (°)	d_1 (Å)	d_2 (Å)	$a/\sqrt{2}$(Å)
0	176.6	2.747	2.832	2.754
3.0	176.8	2.712	2.812	2.762
6.0	176.6	2.717	2.826	2.771
9.0	176.6	2.747	2.832	2.799

higher energy end [8,13]. It is investigated in the literature which orbitals consist this sharp band, doping conducting electrons to be n-type carriers in the crystals. We confirmed that this was composed of 3d orbitals in Ti. This is consistent with the literature which proved that the conduction band bottom was mainly composed of 3d orbitals in Ti [8, 13]. While the conduction bottom was calculated to be at Γ point, the lowest part of the conduction band intersected by Fermi energy level was revealed to be stretched toward the X point direction.

With the calculations of charge transfer between constituent atoms, spatial distribution of charges, and rearrangements of atomic positions around dopants, we can make deduction on the mechanism how to emerge n-type conduction carriers by doping. The calculated L̈owdin charges are compiled in Table 4. Initial charges (number of valence electrons) are Sr: 10.00(4 s: 2.00; 5 s: 2.00; 4p: 6.00); La: 11.00(5 s: 2.00; 6 s: 1.50; 5p: 6.00; 6p: 0.50; 5d: 1.00; 4 f: 0.00); Ti: 12.00(3 s: 2.00; 4 s: 2.00; 3p: 6.00; 3d: 2.00) and O: 6.00(2 s: 2.00; 2p: 4.00), respectively, which are defined in the pseudopotential library files. As discussed in the previous subsection, those calculated for undoped SrTiO$_3$ for U = 9.0 eV were Sr: 8.82; Ti: 10.03; and O: 6.95 as we have seen in Table 2. With La-doping, positivity of Ti atoms decreased by ∼ 0.4 – 0.6 and negativity of O atoms decreased by ∼ 0.2 – 0.3 through transformation of some of the p electrons in O into the d electrons in Ti. Such rearrangements of charge were milder for the larger U. Substitution of Sr by La were replacement of + 1.1 positive ions by + 0.3 – 0.4 positive ions. As we will show later in the charge density plots, La-doping caused decrease in charge density localized around La site compared with those of Sr sites. Although Table 4 indicates that small number of electrons occupied f-orbitals, Fig. 7 shows the effect on the electronic structure of

Table 4
Löwdin charges for the atoms in the relaxed local structure around doped La in La:SrTiO$_3$. Annotations (n) and (d) index atomic positions at neighboring and distant sites of La.

U (eV)		Sr (n)	Sr (d)	La	Ti (n)	Ti (d)	O (n)	O (d)
0	total	8.85	8.85	10.62	10.66	10.66	6.67	6.75
	s	2.17	2.17	2.17	2.26	2.26	1.70	1.72
	p	6.68	6.68	6.67	5.99	5.99	4.97	5.03
	d	0.00	0.00	1.53	2.41	2.41	0.00	0.00
	f	0.00	0.00	0.25	0.00	0.00	0.00	0.00
3.0	total	8.86	8.86	10.64	10.59	10.59	6.70	6.76
	s	2.17	2.17	2.17	2.26	2.26	1.70	1.72
	p	6.69	6.69	6.68	5.99	5.99	5.00	5.04
	d	0.00	0.00	1.53	2.34	2.34	0.00	0.00
	f	0.00	0.00	0.26	0.00	0.00	0.00	0.00
6.0	total	8.87	8.87	10.65	10.51	10.51	6.72	6.79
	s	2.18	2.18	2.18	2.27	2.27	1.71	1.72
	p	6.69	6.69	6.68	5.99	5.99	5.01	5.07
	d	0.00	0.00	1.53	2.25	2.25	0.00	0.00
	f	0.00	0.00	0.26	0.00	0.00	0.00	0.00
9.0	total	8.89	8.89	10.66	10.38	10.38	6.75	6.82
	s	2.19	2.19	2.19	2.27	2.27	1.71	1.72
	p	6.70	6.70	6.69	5.99	5.99	5.04	5.10
	d	0.00	0.00	1.52	2.12	2.12	0.00	0.00
	f	0.00	0.00	0.26	0.00	0.00	0.00	0.00

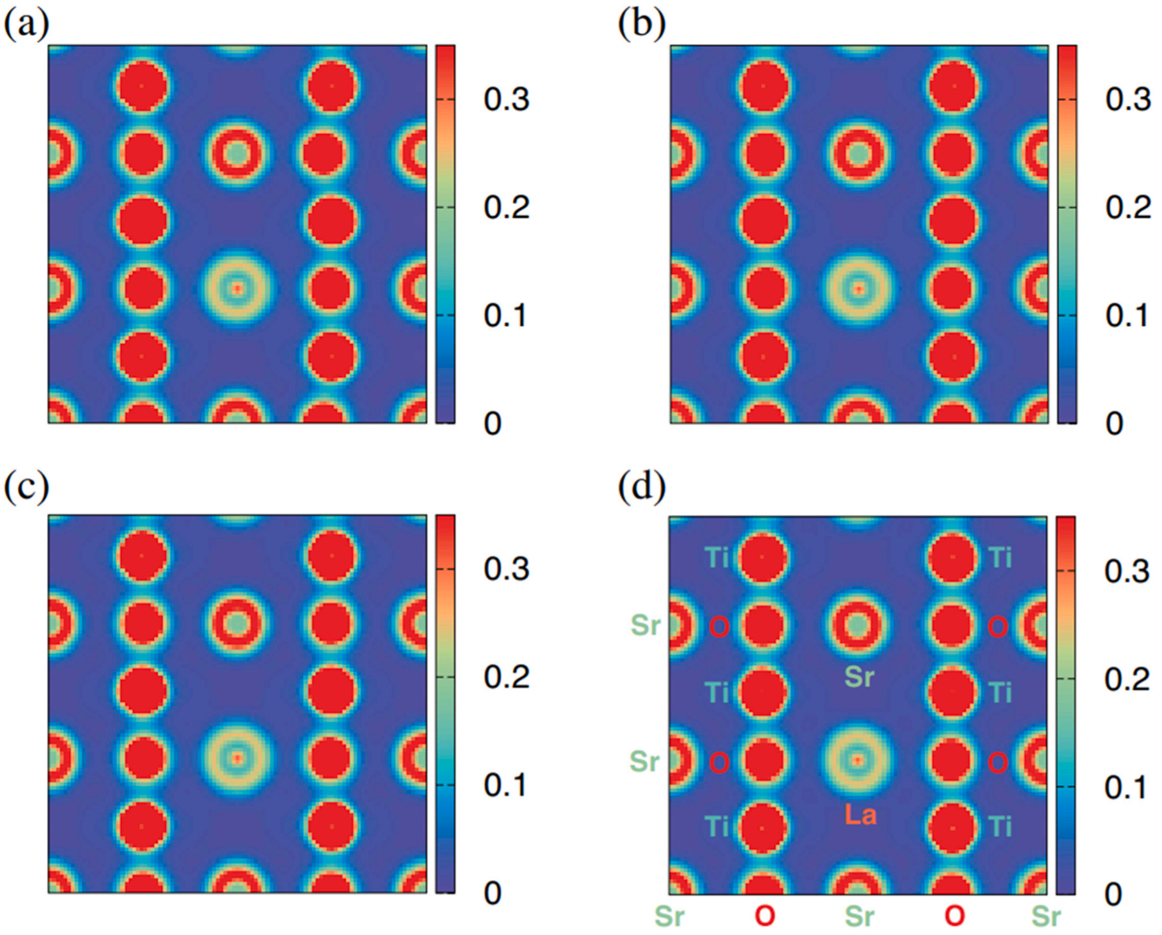

Fig. 8. 2D charge density plots for La:SrTiO$_3$ calculated with DFT+U method plotted for the (110) plane: U = (a) 0, (b) 3.0, (c) 6.0 and (d) 9.0 eV. Atoms are labelled in (d).

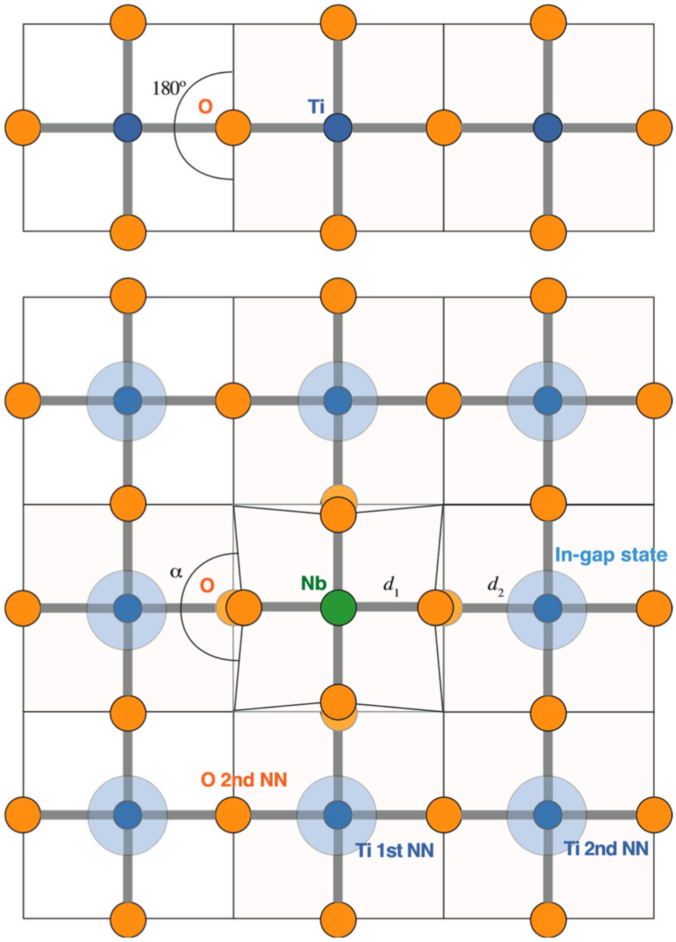

Fig. 9. Schematic for the atomic arrangements in a (002) plane around a Ti replaced by Nb (upper panel) before and (lower panel) after the doping.

the occupied states is negligible.

The 2D charge density plots for La:$SrTiO_3$ calculated with DFT+U method plotted for the (110) plane: U = (a) 0, (b) 3, (c) 6 and (d) 9 eV are shown in Fig. 8. The charge densities presented here are integrated to the number of electrons in each atom. As we see especially in Fig. 8(a), O atoms neighboring Sr, not only those neighboring La, also moved inward when $U = 0$. The Ti-O-Ti angles neighboring Sr reduced to 172.4° for $U = 0$, while they were 179.0° for $U = 3.0$, 178.9° for $U = 6.0$ and 178.9° for $U = 9.0$. As will be described in the next subsection for the Nb-substitution, the smaller distortions near substituted La atom compared with those observed in experiments [8] are likely to be because of the limitation in the simulation cell size.

By introducing the less positive La cations in the crystal, native cations, Sr or Ti, in the matrix crystal should also be less positive. To transfer some of the electrons to Ti atoms, the 3*d* orbitals, which are originally situated at the nearest to the Fermi energy, should be the electron transfer destination. Thus, some of the electrons in O, whose 2*p* electrons are located at the valence band top, are transferred to the Ti 3*d* orbitals, and the Fermi energy level intersects the conduction band bottom, while Ti sites are spatially distanced from La by the presence of distorted O atoms. This is also illustrated in Fig. 5 as in-gap states at Ti sites.

3.3. Calculations for Nb:$SrTiO_3$

As for the Nb:$SrTiO_3$, cubic structure were proved to be stable again. The parameters for the relaxed local structure around dopant Nb defined in Fig. 9 are calculated and compiled in Table 5. The relations of the values, $\alpha < 180°$ and $a/2 < d_1 < d_2$, result from the relaxed atomic arrangements that the O atoms neighboring Nb are attracted toward the dopant Nb atoms, and that the Ti atoms at the nearest neighbors of Nb are repelled away from the dopant. As we will see later in the 2D charge density plots, the (002) and all other equivalent planes of Ti and O are not distorted at Ti site despite the relations above. The cube surrounded by those planes isotropically expands, and its inside shrinks.

The calculated Löwdin charges are compiled in Table 6. Initial charges (number of valence electrons) are Sr: 10.00(4 *s*: 2.00; 5 *s*: 2.00;

Table 5
Parameters for the relaxed local structure around doped Nb in Nb:$SrTiO_3$. The angle (α) and the distances (d_1, d_2) are defined in Fig. 9.

U (eV)	α (°)	d_1 (Å)	d_2 (Å)	$a/2$(Å)
0	179.1	1.962	1.967	1.949
3.0	179.0	1.963	1.974	1.954
6.0	178.8	1.964	1.982	1.961
9.0	178.5	1.968	1.995	1.972

Table 6
Löwdin charges for the atoms in the relaxed local structure around doped Nb in Nb:$SrTiO_3$. Annotations (n) and (d) index atomic positions at neighboring and distant sites of Nb.

U (eV)		Sr (n)	Sr (d)	Nb	Ti (n)	Ti (d)	O (n)	O (d)
0	total	8.81	8.85	12.56	10.71	10.70	6.67	6.74
	s	2.13	2.15	2.25	2.26	2.26	1.67	1.72
	p	6.68	6.70	7.03	5.99	5.99	5.00	5.02
	d	0.00	0.00	3.28	2.46	2.45	0.00	0.00
3.0	total	8.82	8.86	12.50	10.59	10.59	6.64	6.76
	s	2.13	2.15	2.25	2.27	2.27	1.67	1.72
	p	6.68	6.71	7.04	5.99	5.99	4.97	5.04
	d	0.00	0.00	3.21	2.33	2.33	0.00	0.00
6.0	total	8.83	8.87	12.51	10.50	10.49	6.65	6.78
	s	2.14	2.16	2.26	2.27	2.27	1.67	1.72
	p	6.69	6.71	7.04	5.99	5.98	4.98	5.06
	d	0.00	0.00	3.21	2.24	2.24	0.00	0.00
9.0	total	8.84	8.89	12.54	10.41	10.38	6.62	6.82
	s	2.14	2.16	2.25	2.27	2.28	1.65	1.73
	p	6.70	6.73	7.04	5.99	5.99	4.97	5.09
	d	0.00	0.00	3.25	2.15	2.11	0.00	0.00

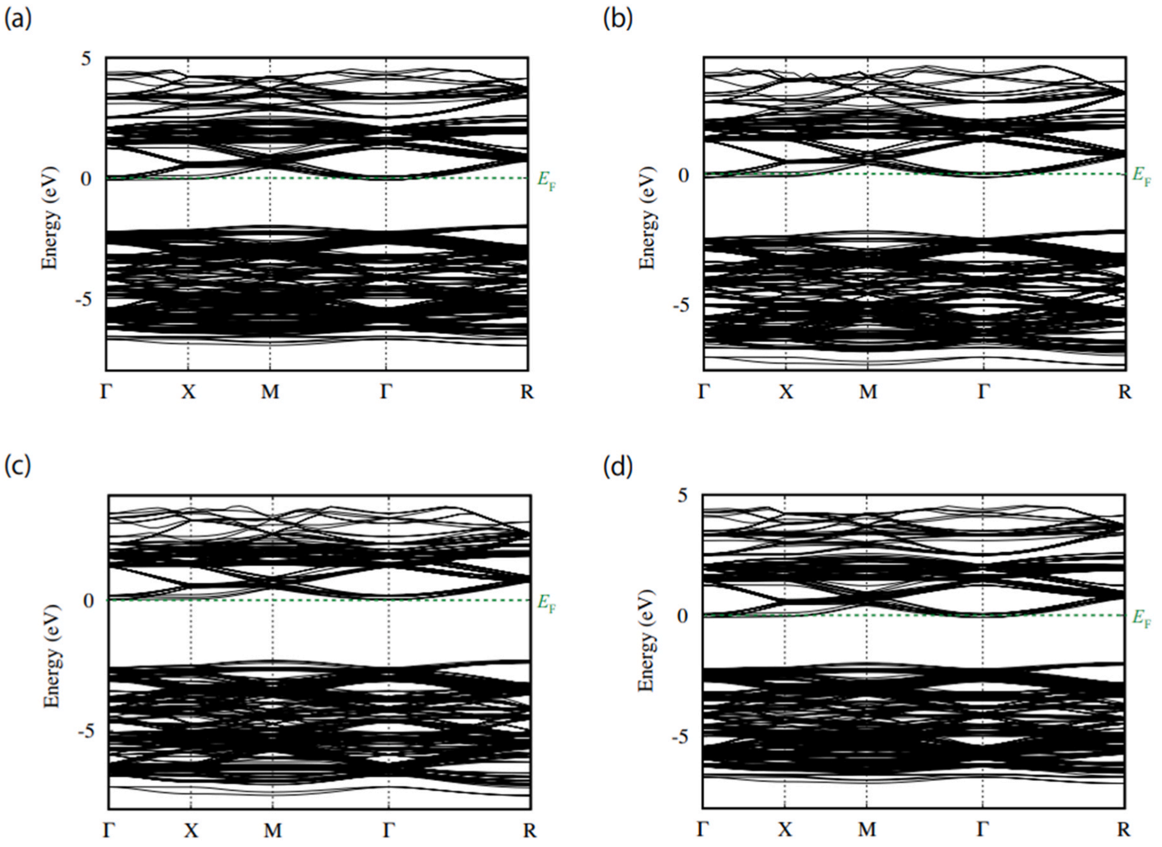

Fig. 10. Band structures for Nb:SrTiO$_3$ calculated with DFT+U method using a simulation box of 3 × 3 × 3 unit cells: U = (a) 0, (b) 3.0, (c) 6.0 and (d) 9.0 eV. Fermi energy (E_F) is set to the origin of energy.

4*p*: 6.00); Nb: 13.00(4 *s*: 2.00; 5 *s*: 2.004*p*: 6.00; 4*d*: 3.00); Ti: 12.00(3 *s*: 2.00; 4 *s*: 2.00; 3*p*: 6.00; 3*d*: 2.00) and O: 6.00(2 *s*: 2.00; 2*p*: 4.00), respectively, which are defined in the pseudopotential library files. As compiled in Table 6, charge rearrangements did not differ so much from La-doping case. With Nb-doping, positivity of Ti atoms decreased by ~ 0.4 – 0.7, and negativity of O atoms decreased by ~ 0.1 – 0.3. Rearrangements of the charges were milder for the larger U. Substitution of Ti by Nb were replacement of + 1.3 –1.5 positive ions by + 0.4 – 0.5 positive ions.

The band structures are given in Fig. 10, and presented in Fig. 11 are the calculated total and partial density of states corresponding to the band structures. A reported calculation for the metallic state of the lightly electron-doped SrTiO$_3$ [36] appeals that the sharp band observed in photoelectron spectroscopy just below the Fermi energy level consists mainly of Ti 3*d* states with a slight hybridization of O 2*p* states. This coincides with the present calculation for U = 9.0 eV, which is shown in Fig. 11 (d), while the partial density of states for O 2*p* is non-zero but small near E_F. In addition, the lowest part of the conduction band intersected by Fermi energy level was stretched toward the X point direction, which was same as the La-doping case. As displayed in Fig. 11, the in-gap states at the conduction band bottom are of Ti 3d orbitals, and consist not only of the first nearest-neighbor Ti, but also of the second and third nearest-neighbor Ti atoms. The isotropic expanding of the cube of the (002) planes and its equivalents including Nb at its center leads to simultaneous repelling of all the 1st, 2nd and 3rd nearest neighbor (NN) Ti atoms away from the substitutional Nb atoms, and corresponds to the emergence of the in-gap states containing the 3*d* orbitals in, not one, but all of these NN Ti atoms. The simultaneous repelling, or isotropic expanding, is also reflected in the 2D charge density plots presented in Fig. 12. Apparently, Nb-doping did not bring about so much modulation in charge density as presented in Fig. 12. As a consequence, intrusion of Fermi energy level into conduction-band density of states, and atomic rearrangements near Nb substitutional defects, were milder than those in La-substitution, even though we have used a larger simulation cell for the Nb-substitution. The rearrangements are concentrated in the single unit cell containing the dopant, and the Fermi energy level intrude into the conduction bands of the Ti-O planes outside the cell not containing the dopants. Nevertheless, the small rearrangements in atomic positions are still because of our simulation cell size. The present small shrinkage around Nb comes from a partial offset of an attractive force acting on O atom from the neighboring Nb atoms by another attractive force from another Nb located outside the simulation box toward opposite direction under periodic boundary condition. In our 3 × 3 × 3 unit-cell simulation box, the unit cell at the center containing O atoms shifted toward the substituted Nb are located in the expanded cubic cage of the (002) planes and its equivalents composed of the Ti-O network. In order to describe the lattice relaxation of these planes, we need 3 × 3 × 3 unit cells as the minimum, because another Nb-substituted cell generated by the periodic boundary condition does not contact directly at the planes with that size. As a proof of it, if we calculate with 2 × 2 × 2 simulation box, the balance of the attractive forces between two toward opposite directions is exactly held at the (002) plane, and variation of the angle α from 180° disappears at the same time. Consequently, it is probable that the twist

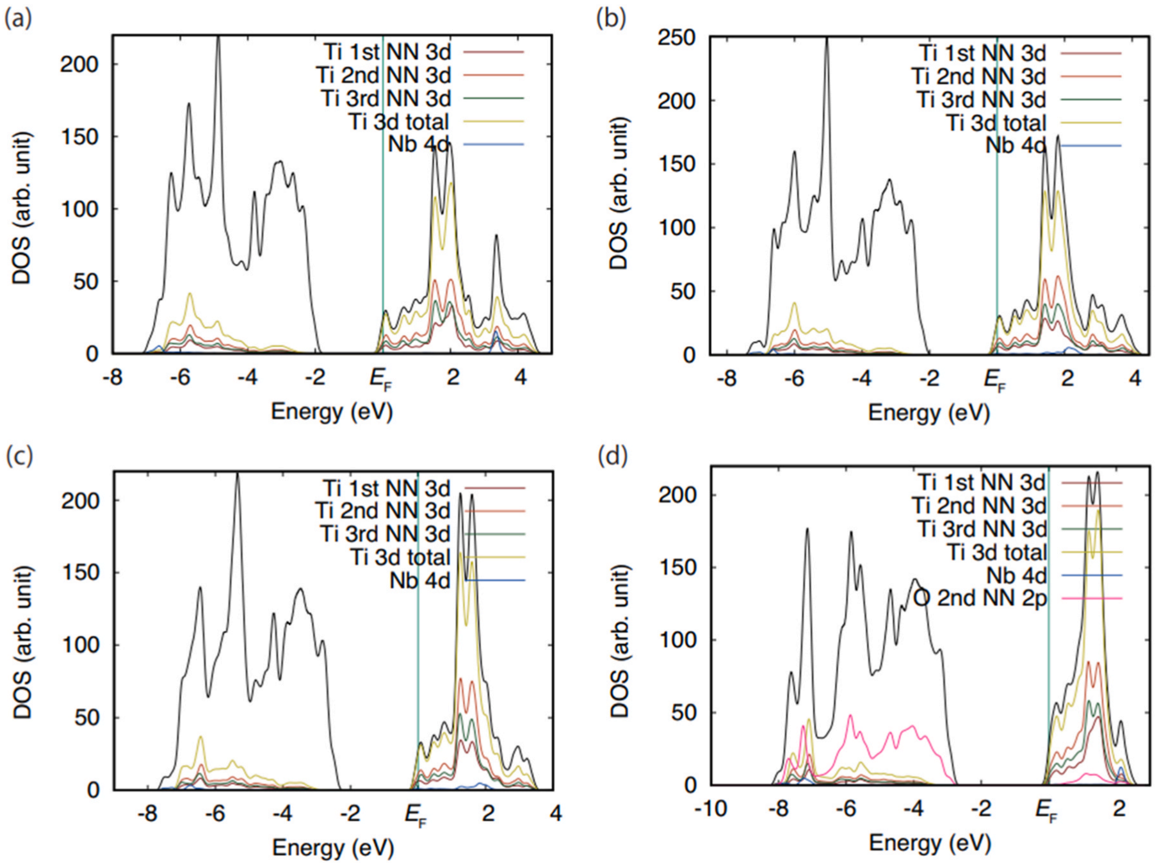

Fig. 11. Total and partial density of states for Nb:SrTiO$_3$ calculated with DFT+U method using a simulation box of 3 × 3 × 3 unit cells: U = (a) 0, (b) 3.0, (c) 6.0 and (d) 9.0 eV. The 1st and 2nd nearest neighbor (NN) positions are defined in Fig. 9, and the 3rd NN positions are defined as the remaining Ti sites in the cube consists of the (002) planes and their equivalents. Total density of states is drawn in solid black line, and partial density of states are labeled in legend.

at angle α can be more sharp if we calculate with a larger periodicity. The minimum size supercell in this sense for the La-substituted cell is composed of 2 × 2 × 2 unit cells.

The result that the sharp band just below the Fermi level consists of the isotropic expanding cube of the (002) planes of Ti-O and its equivalents around the substitutional Nb also means that the carriers doped in n-type does not need to transport across the electronic states containing the Nb defects. The doped electron carriers can conduct within Ti-O network without scattering by defects. Therefore, the substitution of Ti with Nb is not inferior to that of Sr with La, although the Nb dopants are embedded in the Ti-O network while Sr is not contained in the network. As replacing Sr by La does not disturb the n-type carrier transportation within Ti-O conduction planes, Nb doping forms the conduction path which bypasses the unit cell containing the dopants. Taking the mild alternation of the local atomic arrangements also into account, Nb:SrTiO$_3$ is as appopriate as La:SrTiO$_3$ for an n-type semiconductor, which is confirmed in the experiments [37].

4. Conclusion

First-principles calculations with DFT+U were performed on the local structures and the in-gap electronic states of n-type SrTiO$_3$ introduced by substitution of Sr by La or Ti by Nb.

Preliminary calculations for the undoped SrTiO$_3$ revealed that the direct and indirect energy gaps in the band structures were better reproduced by assigning a large U on Ti.

For La-doped SrTiO$_3$, cubic structures, $a = c$, were proved to be stable by the structural relaxation calculations, even though the tetragonal structures were assumed for the unit cell. The O atoms neighboring the substitutional La slightly moved toward the dopants. The sharp electron band, which gave n-type conductivity and resulted from the intersection of Fermi energy level at the conduction band bottom with La-doping, was composed of 3d orbitals in Ti. The La-doping transformed some of the p electrons in O into the d electrons in Ti, which contributed to n-type conduction.

For Nb-doped SrTiO$_3$, cubic structure were proved to be stable again. The local structure around the Nb substitutional dopants to Ti was revealed that the O atoms neighboring the dopants were attracted toward the Nb atoms, while the Ti atoms at the nearest neighbors of the dopants were repelled away from the Nb atoms. The sharp band of the in-gap states just below the Fermi energy was not only of the first nearest-neighbor Ti atoms, but also of the second and third nearest-neighbor Ti atoms of the Nb dopants. The degree of Fermi energy level intrusion into conduction band and atomic rearrangements near Nb substitutional defects were milder than those of La substitutions.

Replacement of Sr by La not contained in Ti-O network does not disturb the electron transport within Ti-O conduction planes. Similarly, Nb-doping in Ti site does not interrupt the n-type carrier transportation through conduction path formation which bypasses the unit cell containing the dopants.

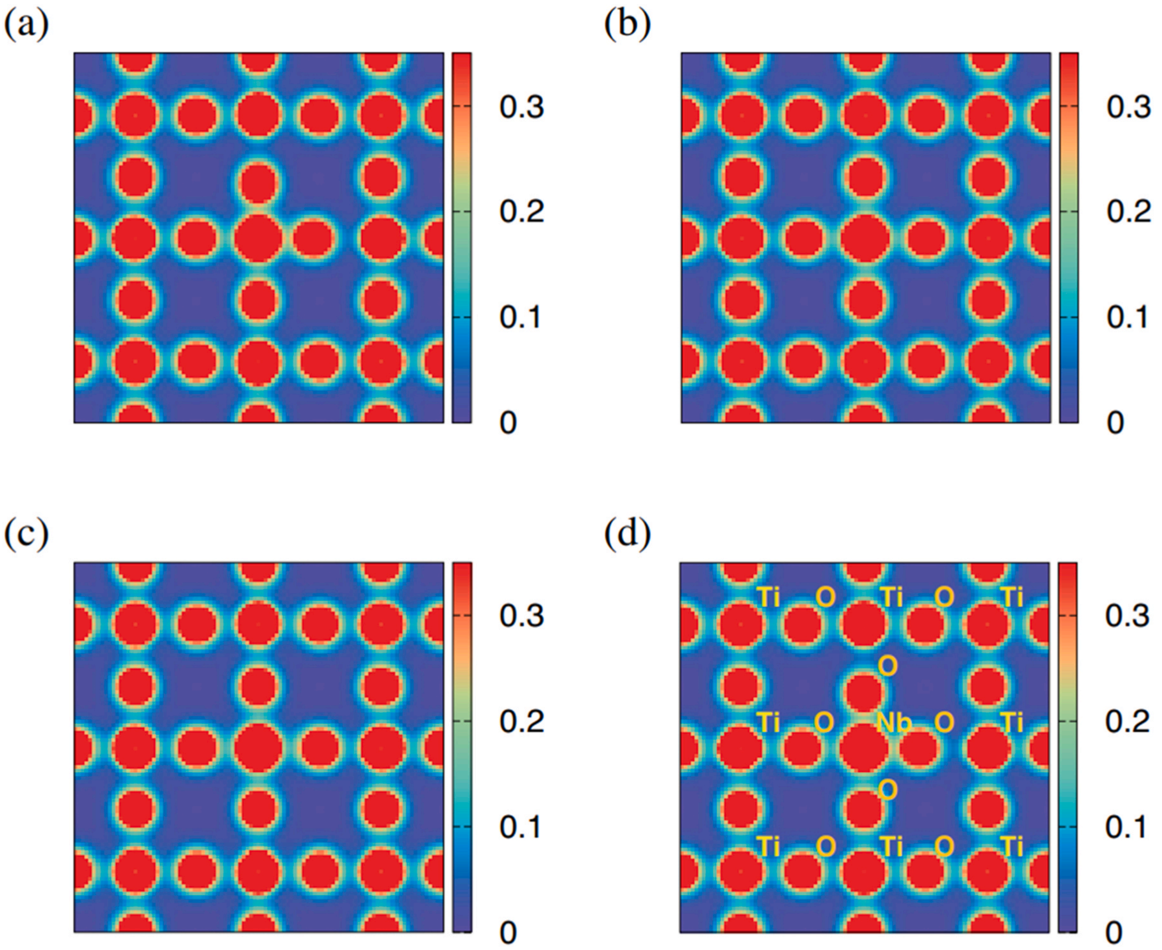

Fig. 12. 2D charge density plots for Nb:SrTiO$_3$ calculated with DFT+U method plotted for the (002) plane: U = (a) 0, (b) 3.0, (c) 6.0 and (d) 9.0 eV.

Declaration of Competing Interest

We declare that we have no conflicts of interest to disclose. We have no known competing financial interests or personal relationships that could have appeared to influence the work reported in this article.

Acknowledgment

We acknowledge Ryo Sakaguchi who arranged some of the hardwares used for the present computation.

References

[1] Y. Yamada, Y. Kanemitsu, J. Appl. Phys. 109 (2011), 102410.
[2] M. Bibes, J.E. Villegas, A. Barthélémy, Adv. Phys. 60 (2011) 5.
[3] S.S. Jana, T. Maiti, ACS Appl. Mater. Interfaces 14 (2022) 14174.
[4] N. Tsvetkov, B.C. Moon, J. Lee, J.K. Kang, ACS Appl. Energy Mater. 3 (2020) 344.
[5] C. Jia, Y. Ren, Y. Yin, W. Zhang, Appl. Phys. Lett. 115 (2019), 223503.
[6] Y.S. Kim, S.M. Hwang, C. Yoon, J.H. Lee, J. Jeon, T. Choi, B.H. Park, Appl. Phys. Lett. 116 (2020), 022901.
[7] Z. Ma, L. Li, Y. Wang, P. Zhou, Y. Guo, Y. Liu, K. Liang, Y. Qi, T. Zhang, Appl. Phys. Lett. 116 (2020), 032903.
[8] Y. Aiura, K. Ozawa, Y. Tezuka, M. Minohara, A. Samizo, K. Bando, H. Kumigashira, K. Mase, Phys. Chem. Chem. Phys. 21 (2019) 14646.
[9] Y. Aiura, K. Ozawa, E.F. Schwier, K. Shimada, K. Mase, J. Phys. Chem. C. 122 (2018) 19661.
[10] Y. Yamada, Y. Kanemitsu, Thin Solid Films 520 (2012) 3843.
[11] C. Ricca, I. Timrov, M. Cococcioni, N. Marzari, U. Aschauer, Phys. Rev. Res. 2 (2020), 023313.
[12] W. Wunderlich, H. Ohta, K. Koumoto, Phys. B 404 (2009) 2202.
[13] (a) Y. Aiura, H. Bando, I. Hase, Y. Nishihara, Y. Haruyama, T. Shimizu, H. Suzuki, J. Electron Spectrosc. Rel. Phenom. 78 (1996) 199;
(b) Y. Aiura, H. Bando, I. Hase, Y. Nishihara, Y. Haruyama, H. Suzuki, Superlattices Microstruct. 21 (1997) 321.
[14] C. Rodenbücher, A. Jauß, V. Havel, R. Waser, K. Szot, Phys. Status Solidi RRL 8 (2014) 781.
[15] R. Liang, D.A. Bonn, W.N. Hardy, Phys. Rev. B 73 (2006), 180505 (R).
[16] P. Giannozzi, S. Baroni, N. Bonini, M. Calandra, R. Car, C. Cavazzoni, D. Ceresoli, G.L. Chiarotti, M. Cococcioni, I. Dabo, A.D. Corso, S. de Gironcoli, S. Fabris, G. Fratesi, R. Gebauer, U. Gerstmann, C. Gougoussis, A. Kokalj, M. Lazzeri, L. Martin-Samos, N. Marzari, F. Mauri, R. Mazzarello, S. Paolini, A. Pasquarello, L. Paulatto, C. Sbraccia, S. Scandolo, G. Sclauzero, A.P. Seitsonen, A. Smogunov, P. Umari, R.M. Wentzcovitch, J. Phys.: Condens. Matter 21 (2009), 395502.
[17] P. Giannozzi, O. Andreussi, T. Brumme, O. Bunau, M. Buongiorno Nardelli, M. Calandra, R. Car, C. Cavazzoni, D. Ceresoli, M. Cococcioni, N. Colonna, I. Carnimeo, A. Dal Corso, S. de Gironcoli, P. Delugas, R.A. Distasio, A. Ferretti, A. Floris, G. Fratesi, G. Fugallo, R. Gebauer, U. Gerstmann, F. Giustino, T. Gorni, J. Jia, M. Kawamura, H.-Y. Ko, A. Kokalj, E. Küçükbenli, M. Lazzeri, M. Marsili, N. Marzari, F. Mauri, N.L. Nguyen, H.-V. Nguyen, A. Otero-de-la-Roza, L. Paulatto, S. Poncé, D. Rocca, R. Sabatini, B. Santra, M. Schlipf, A.P. Seitsonen, A. Smogunov, I. Timrov, T. Thonhauser, P. Umari, N. Vast, X. Wu, S. Baroni, J. Phys.: Condens. Matter 29 (2017), 465901.
[18] (a) J. Perdew, Phys. Rev. Lett. 55 (1985) 1665;
(b) J. Perdew, Phys. Rev. Lett. 55 (1985) 2370.
[19] A.I. Lichtenstein, J. Zaanen, V.I. Anisimov, Phys. Rev. B 52 (1995) R5467.
[20] V.I. Anisimov, F. Aryasetiawan, A.I. Lichtenstein, J. Phys.: Condens. Matter 9 (1997) 767.
[21] ⟨http://pseudopotentials.quantum-espresso.org/legacy_tables/ps-library⟩.

[22] (a) P.E. Bröchl, Phys. Rev. B 50 (1994) 17953;
(b) G. Kresse, D. Joubert, Phys. Rev. B 59 (1999) 1758.

[23] J.P. Perdew, A. Ruzsinsky, G.I. Csonka, O.A. Vydrov, G.E. Scuseria, L. A. Constantin, X. Zhou, K. Burke, Phys. Rev. Lett. 100 (2008), 136406.

[24] J. Perdew, K. Burke, M. Ernzerhof, Phys. Rev. Lett. 77 (1996) 3865.

[25] ⟨https://www.quantum-espresso.org/Doc/INPUTPW.html⟩.

[26] H.J. Monkhorst, J.D. Pack, Phys. Rev. B 13 (1976) 5188.

[27] K. van Benthem, C. Elsässer, R.H. French, J. Appl. Phys. 90 (2001) 6156.

[28] A. Janotti, B. Jalan, S. Stemmer, C.G. Van de Walle, Appl. Phys. Lett. 100 (2012), 262104.

[29] S. Ahmed, T. Hasan, A.K.M.S.H. Faysal, S.S. Nishat, M.N.I. Khan, A. Kabir, I. Ahmed, Comput. Mater. Sci. 214 (2022), 111743.

[30] A. Chen, S.V. Nair, B. Miljkovic, C. Souza, H.E. Ruda, Z. Ji, J. Nanopart. Res. 22 (2020), 259.

[31] Y. Duan, P. Ohodnicki, B. Chorpening, G. Hackett, J. Solid State Chem. 256 (2017) 239.

[32] X. Han, K. Song, L. Lu, Q. Deng, X. Xia, G. Shao, J. Mater. Chem. C. 1 (2013) 3736.

[33] A. Kinaci, C. Cevik, T. C¸ağin, Phys. Rev. B 82 (2010), 155114.

[34] P.-O. Löwdin, J. Chem. Phys. 18 (1950) 365.

[35] T. Kar, A.B. Sannigrahi, J. Mol. Struct. 165 (1987) 47.

[36] Y. Aiura, I. Hase, H. Bando, T. Yasue, T. Saitoh, D.S. Dessau, Surf. Sci. 515 (2002) 61.

[37] S. Ohta, T. Nomura, H. Ohta, K. Koumoto, J. Appl. Phys. 97 (2005), 034106.